

## **SIMULATION OF TORPEDO ANCHOR INSTALLATION USING THE MATERIAL POINT METHOD**

**Leonardo Tolêdo Ferreira**

*contato@leonardotoledo.org*

*Undergraduate Student, Center of Technology, Federal University of Alagoas*

**Adeildo Soares Ramos Júnior**

*adramos@lccv.ufal.br*

*Associate Professor, Center of Technology, Federal University of Alagoas*

**Tiago Peixoto da Silva Lôbo**

*tiago@lccv.ufal.br*

*Researcher, Laboratory of Scientific Computing and Visualization*

*Av. Lourival Melo Mota, S/N, Tabuleiro do Martins, 57072-900, Maceió/AL, Brazil*

**Ricardo Garske Borges**

*garske@petrobras.com.br*

*Researcher, Ocean Engineering Technology, PETROBRAS/CENPES*

*Av. Horácio Macedo, 950, Cidade Universitária, 21941-915, Rio de Janeiro/RJ, Brazil*

**Abstract.** Exploration of deep-sea reservoirs is an important industrial activity due to the amount of oil and gas the modern society demands. Thus, one needs to find a safe way to moor ships and platforms and ensure continued and uninterrupted distribution of oil and gas. Torpedo anchors are often used as foundation for offshore facilities as they are cost effective and their usage is independent of water depth. As it is not easy to predict the behavior of installing such structures, usage of a numerical tool is necessary and this theme has been the focus of many studies, aided by numerical methods such as Computational Fluid Dynamics (CFD), Discrete Element Method (DEM) and Material Point Method (MPM). The last of these, the MPM uses an interesting strategy that benefits from both Lagrangian and Eulerian formulations. For instance, the convective term in momentum conservation is eliminated as a consequence of the Lagrangian formulation and mesh distortion is avoided by a fixed background grid. On the MPM, material information is placed inside material points, which are used to interpolate data to the background grid, where the equations of motion are solved. Since the grid is fixed, large strains and displacements are not a problem. Many authors used an axisymmetric formulation to simulate the installation of torpedo anchors with the MPM. In real-life situations, however, the soil might display asymmetries. Therefore, this work adopts the usual non-symmetric formulation to simulate the installation of two different anchor designs on a non-symmetric soil using the MPM.

**Keywords:** Torpedo anchor, Material point method, Anchor design, Non-symmetry, Elastoplasticity

## 1 Introduction

Torpedo anchors have been used by Petrobras since 1996 to support floating offshore structures (Medeiros Júnior [1]). They are no more than normal steel piles, which are released in free fall to find an underwater soil on which to moor these facilities.

According to Bezerra [2], this sort of anchor has fit well to the needs of the Petrobras since, in deep waters, it is easy to find very soft clays, which torpedo anchors handle very well. Besides, they are a cheap alternative to traditional mooring systems.

In practice, however, these anchors are submitted to the force of the waters and can have their course changed during installation. Knowing beforehand the embedment depth these anchors are going to achieve and the soil irregularities that might deviate them during installation is of vital importance.

Given the relevance of these anchors in offshore engineering and the necessity to simulate their behavior, many authors have simulated the installation of such structures with the aid of numerical tools in the likes of the discrete element method (Carvalho Júnior et al. [3]), the finite element method (Sousa et al. [4]), Lagrangian-Eulerian finite element analysis (Nazem et al. [5]) and the material point method (Al-Kafaji [6]).

The last of these methods, the material point method (MPM) is the focus of the simulations in this article. The Material Point Method (MPM) was proposed by Sulsky et al. [7] as an extension of a particle-in-cell (PIC) method. In the MPM, a continuum domain is discretized into particles or material points (as showed in Figure 1), which are the repositories of material data. The way MPM works is by making interpolations between these particles and a fixed background mesh, as will be further developed on this article.

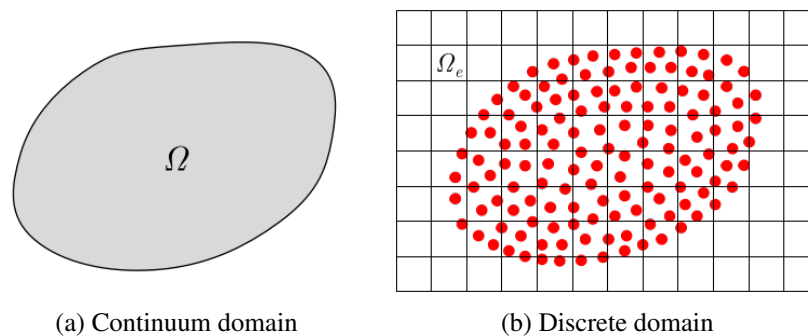


Figure 1. Space discretization on MPM

Figure 2 shows a brief description of what happens during a MPM time step, divided into four simple steps. Firstly, material information that was stored in the particles is mapped to the nodes of the mesh (Fig. 2a). Then, the equations of motion are solved on the nodes (Fig. 2b). Node data are used to calculate particle stresses, by mapping information from the nodes to the particles (Fig. 2c). Finally, particle velocities and positions are updated (Fig. 2d). The process is repeated until the end of the simulation.

The fixed background mesh on which these mappings are done is actually a Lagrangian mesh, but, since node position is never updated (position information is stored in the particles), the mesh remains fixed throughout the simulation. One consequence of this is that the mesh must encompass all the possible locations that the material points may occupy during the simulation. But, as an advantage, mesh distortion is prevented, which makes the MPM a very powerful tool to simulate large strain and large displacement problems.

To simulate the installation of torpedo anchors, Al-Kafaji [6] and Jassim et al. [8] have applied an axisymmetric formulation together with the MPM. In real-life situations, however, the soil might display non-symmetries that could affect the behavior of the torpedo anchor. That way, this article aims to successfully simulate the installation of torpedo anchors using the MPM, and do so with two different torpedo anchor designs in the presence of a non-symmetric soil interface.

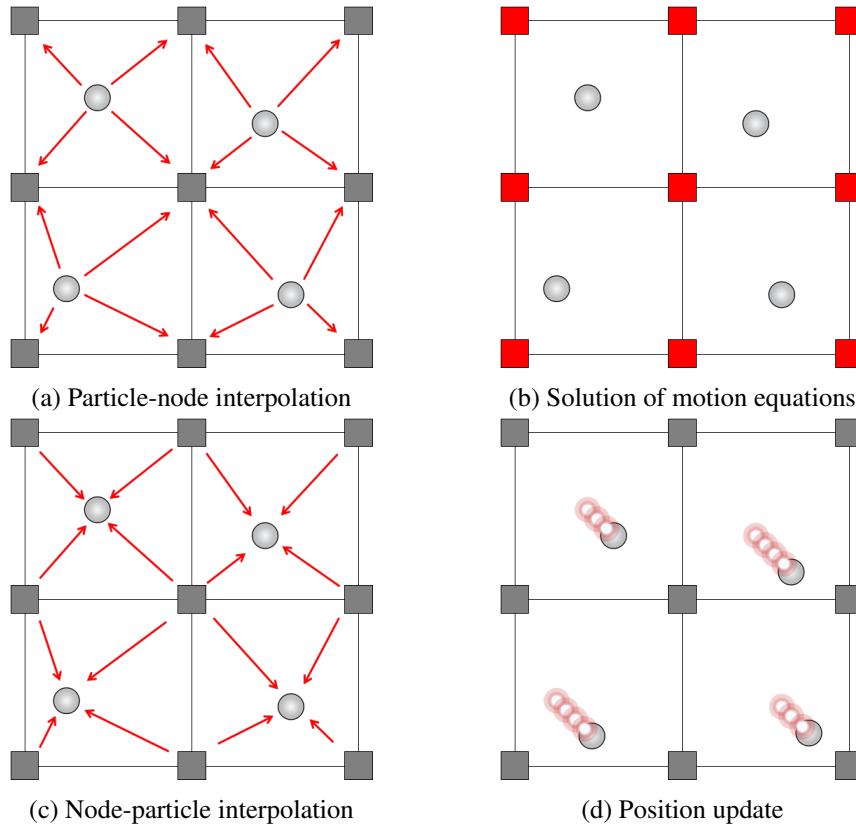


Figure 2. The four basic steps in a simulation with MPM

## 2 Formulation

In this section, the mathematical formulation which is the basis of this article is briefly discussed, following three essential aspects: the general formulation of MPM, the contact algorithm and the elasto-plastic model.

### 2.1 Material point method

MPM is built upon the conservation of momentum (Eq. (1)), since conservation of mass is already met as the mass of the particles is constant through the entire simulation (Andersen and Andersen [9]) and conservation of energy is met as a consequence of mass and momentum conservation being satisfied in a system on which heat exchange is negligible (Zhang et al. [10]).

$$\rho \frac{\partial v_i}{\partial t} = \frac{\partial \sigma_{ij}}{\partial x_j} + \rho g_i, \quad (1)$$

in which,

$\rho$ : mass density,

$v_i$ : velocity field,

$t$ : time,

$\sigma_{ij}$ : Cauchy stress tensor,

$x_j$ : current position vector,

$g_i$ : field force (gravity, in this particular case).

Similarly to what occurs in the finite element method (FEM), conservation of momentum can be written into a weak form. This form takes advantage of dividing the boundary of the domain into two

sections: a boundary on which tractions are prescribed and a boundary on which displacements are prescribed. With usage of an arbitrary weight function and the application of Gauss' theorem and Reynolds' transport theorem, the weak form leads to an equation of lower order than the equation of conservation of momentum. Furthermore, since the mass of the system will be concentrated on the material points (or particles), the mass density can be rewritten as a sum of the mass ( $m_p$ ) of each particle  $p$  in terms of the Dirac delta map ( $\delta$ ):

$$\rho(\mathbf{x}, t) = \sum_p m_p \delta(\mathbf{x} - \mathbf{X}_p), \quad (2)$$

in which,

$\mathbf{X}_p$  = particle position,

With the application of the Dirac delta map in substitution of the mass density in the weak form and after the discretization of the continuum in space (by making use of a fixed background mesh of finite elements) and time (with a time integration scheme), the general equation of the MPM can be written – with the application of a lumped mass matrix – as the following equation of motion (for each node  $n$  of the background mesh in the time step  $i$ ):

$$M_n^i \mathbf{a}_n^i = \mathbf{f}_n^{ext,i} - \mathbf{f}_n^{int,i}, \quad (3)$$

in which,

$M_n^i = \sum_p m_p N_n^e(x_p^i)$ : nodal mass (obtained by interpolating the masses of particles in adjacent elements, using the shape function of node  $n$  in the respective element  $e$  ( $N_n^e$ )),

$\mathbf{a}_n^i$ : nodal acceleration (the unknown in the equation of motion),

$\mathbf{f}_n^{ext,i} = \sum_p m_p \mathbf{g} N_n^e(x_p^i)$ : external nodal force (in this case, gravity, so it corresponds to the weight),

$\mathbf{f}_n^{int,i} = \sum_p V_p \boldsymbol{\sigma}_p^i \cdot \nabla N_n^e(x_p^i)$ : internal nodal force (depends on the particle stress ( $\boldsymbol{\sigma}_p^i$ ) and the particle volume ( $V_p$ )).

The time integration scheme adopted in this article is the Euler method, which is an explicit time integration scheme and, therefore, demands the definition of a critical time step ( $\Delta t_{critical}$ ), which must not, by all means, be surpassed during the simulation:

$$\Delta t_{critical} = \frac{\Delta x}{\sqrt{\frac{E}{\rho}}}, \quad (4)$$

in which,

$\Delta x$ : element size on the fixed background mesh,

$E$ : elastic modulus of the material.

Since the internal nodal forces depend on particle stresses, the moment on which stresses are updated, i.e., before or after solving the equation of motion in a given time step, interferes in the results. On his paper, Bardenhagen [11] talks about two different solutions: *Update Stresses Last* (USL) and *Update Stresses First* (USF). As the name implies, in USF the stresses are updated after solving the equation of motion, whilst in USL the stresses are updated before. USF is a conservative algorithm, but can increase the energy level in some situations. This article adopts the *Modified Update Stresses Last* (MUSL) algorithm, which is a variation of USL that ensures that stresses are updated with nodal velocities from the current time step. The MUSL algorithm is summarized in Fig. 3.

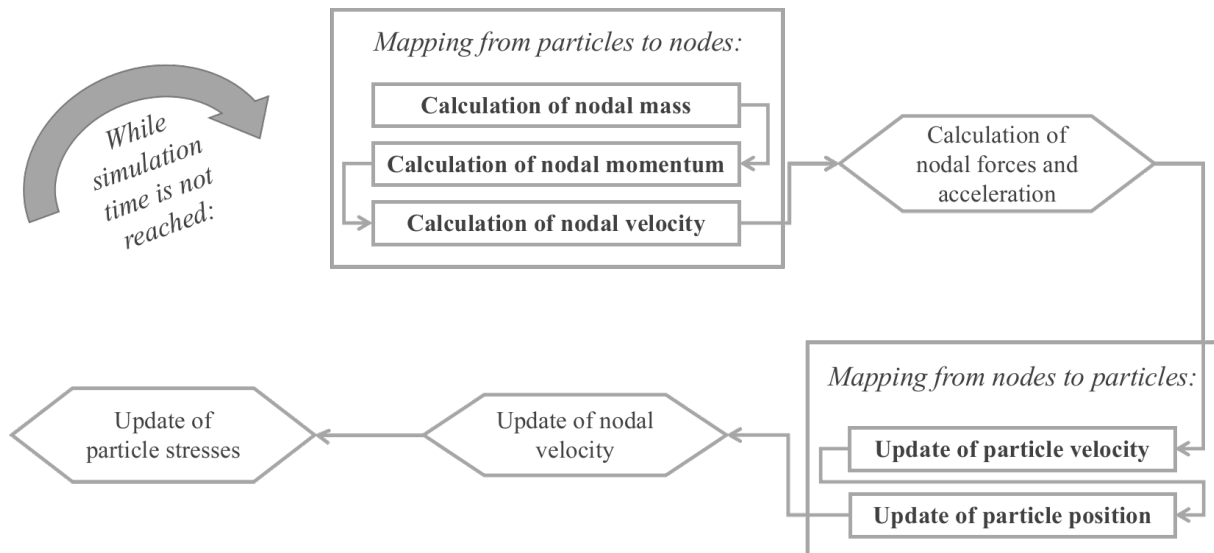


Figure 3. Flowchart of the MUSL algorithm

## 2.2 Contact algorithm

In the MPM, contact is detected not on the particles, but on the nodes of the background grid. MPM handles no-slip contact automatically, as the velocity field of the particles is single-valued and, in consequence, no interpenetration is allowed (York et al. [12]). However, handling only the normal contact is not enough to simulate the installation of torpedo anchors, as the soil on the contact interface gets locked to the anchor and is pulled with it.

That way, a dedicated algorithm to handle the tangential contact is necessary. The approach adopted in this article is similar to the traditional FEM master-slave algorithm. In this approach, three different grids are used: a master grid, containing both bodies 1 (the torpedo anchor) and 2 (the soils), the first slave grid, containing only the anchor and the second slave grid, containing only the soil, as showed in Fig. 4. When the algorithm detects that, in adjacent elements, particles from slave 1 and slave 2 are present, then, the contact happens.

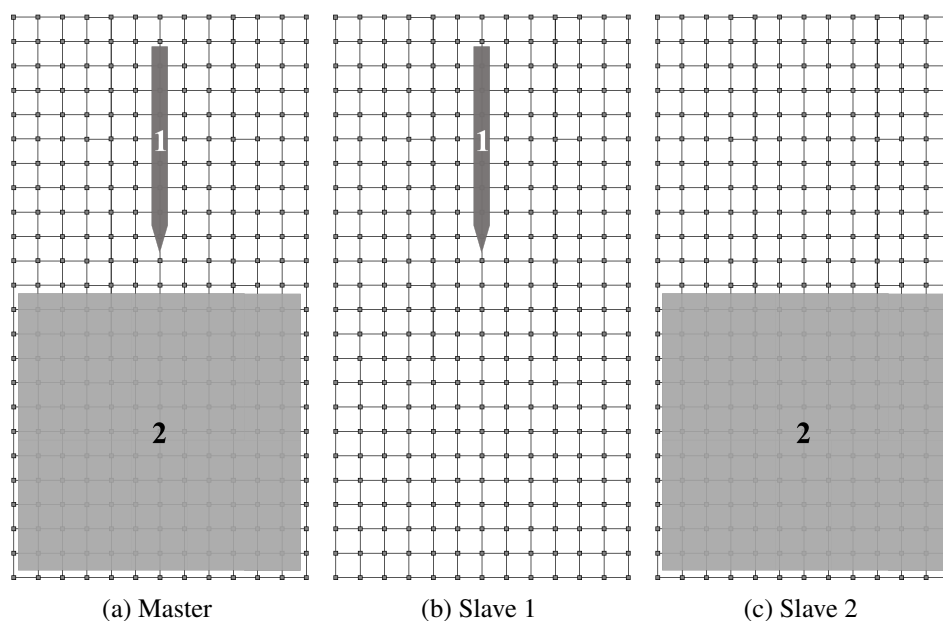


Figure 4. Master and slave meshes for the contact algorithm

### 2.3 Elastoplasticity

In this work, a 2-dimensional analysis is presented, with a plane strain state. The elastic behavior of the materials is assumed to be linear elastic and the von Mises yield criterion is used for plasticity. This formulation was implemented in this work based on the book written by Souza Neto et al. [13].

### 3 Simulation template

Two templates were developed for the simulations in this article. Both templates share the same materials, sizes and mesh properties. The only difference that takes them apart is the anchor design. In template 1, the torpedo anchor doesn't have a fin, while in template 2 the torpedo anchor has a fin. An illustration of the mesh (which doesn't correspond to the real mesh that was simulated in this article) is presented for both templates, as well as the supports in Fig. 5.

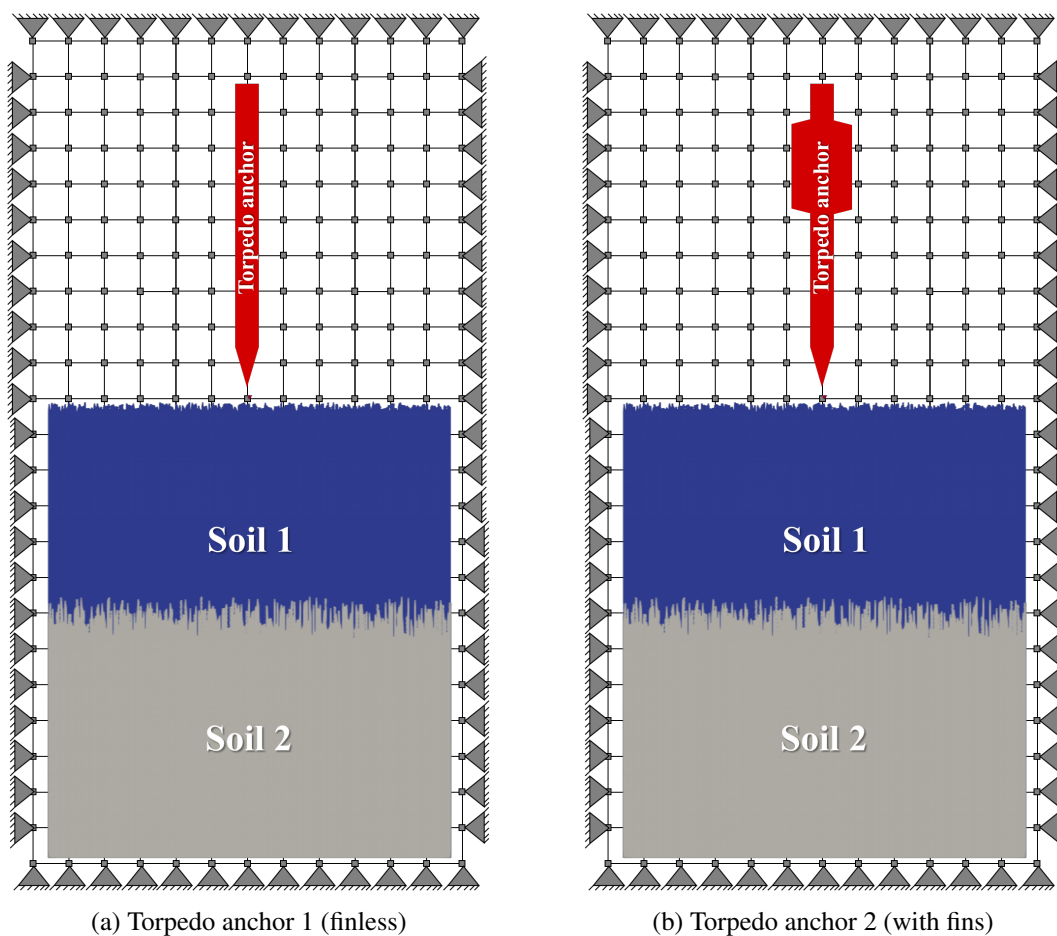


Figure 5. Torpedo anchor templates

Tables 1 and 2 show, respectively, the geometric properties and the materials of the simulations. Figure 6 and Table 3 show the geometric properties of the torpedo anchors. They were the same for both templates, except by the fins, which are in the second template, but not in the first one. The materials adopted here were A36 steel (for both anchors) and two different clay soils (soil data was adapted from Awwad and Al Kodsi [14]). The numerical domain was the same for both simulations, with the exception of the number of particles in template 2, which was bigger as a consequence of the presence of fins.

Table 1. Material properties

	<b>A36 Steel</b>	<b>Clay 1</b>	<b>Clay 2</b>
<b>Density (<math>\rho</math>)</b>	7,800 kg/m <sup>3</sup>	1,500 kg/m <sup>3</sup>	1,700 kg/m <sup>3</sup>
<b>Elastic modulus (<math>E</math>)</b>	$2 \times 10^{11}$ Pa	$5 \times 10^7$ Pa	$4.9 \times 10^7$ Pa
<b>Poisson's ratio (<math>\nu</math>)</b>	0.26	0.2	0.2
<b>Yield stress (<math>\sigma_y</math>)</b>	$2.5 \times 10^8$ Pa	$6 \times 10^3$ Pa	$3 \times 10^3$ Pa

Table 2. Numerical domain properties

<b>Template</b>	<b>Torpedo anchor 1</b>	<b>Torpedo anchor 2</b>
Element size	0.05 m	0.05 m
Number of nodes	243,412	243,412
Number of elements	242,305	242,305
Number of particles	182,742	190,631
% of critical $\Delta t$	10 %	10 %
Simulation time	1s	1s

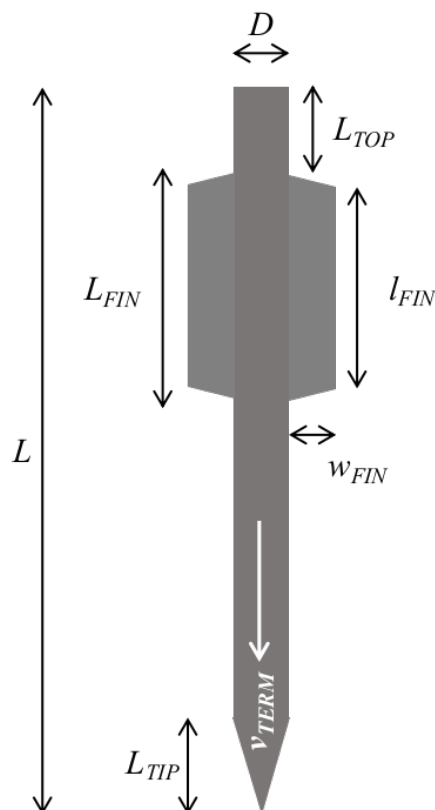


Figure 6. Torpedo anchor geometric elements

Table 3. Geometry specifications

Template element	Torpedo anchor 1 (finless)	Torpedo anchor 2 (with fins)
Full length ( $L$ )	12 m	12 m
Tip length ( $L_{TIP}$ )	1.5 m	1.5 m
Diameter ( $D$ )	0.75 m	0.75 m
Distance from the fin to the top ( $L_{TOP}$ )	–	1 m
Fin's smaller side ( $l_{FIN}$ )	–	3 m
Fin's larger side ( $L_{FIN}$ )	–	5 m
Fin width ( $w_{FIN}$ )	–	0.625 m
Terminal velocity ( $v_{TERM}$ )	30 m/s	30 m/s
Soil height \ width	27 m \ 15 m	27 m \ 15 m

## 4 Results

Figure 7 shows the results of the simulation for both torpedo anchor templates (with and without fins) for different time steps (0, 0.15, 0.30 and 0.45 s). At each time step, torpedo anchor 1 is the one in the left (Figs. 7a, 7c, 7e and 7g) and torpedo anchor 2 is the one in the right (Figs. 7b, 7d, 7f and 7h). Both anchors are launched with a separation of 5 elements to the soil and with terminal velocity ( $v_{TERM}$ ). Figure 8 shows a comparison of the velocities of both torpedo anchors for the time interval between 0 and 0.5 s.

## 5 Conclusion

The MPM was able to successfully simulate the installation of torpedo anchors with a non-symmetric formulation and with two layers of non-symmetric soil, even though a poorly refined mesh of Q4 elements was used due to the computational cost of using more refined meshes and smaller time steps. As explained in the section 2.2, the MPM contact is handled in the nodes and, therefore, the smaller the elements, the closer the bodies in contact get to each other and more precise is the result.

As the results in Fig. 8 show, torpedo anchor 2 (the one with fins) gets down faster than torpedo anchor 1, which was to be expected, since it is a very common design in the industry and it is heavier than torpedo anchor 1. That comes to show that the weight and the aerodynamics of this model would theoretically provide a faster installation according to the simulations hereby presented, but, since the difference was not too significant, more precise simulations would need to be done.

Besides, the results could have been even better if a more refined background mesh was used – informed by smaller time steps – and if the Drucker-Prager yield criterion was adopted instead of the von Mises criterion, which is pressure insensitive and, therefore, optimal for metal simulations, but not for soils [13]. Also, absorbing boundary conditions could have been applied, besides usage of a 3-dimensional simulation template, which is more accurate to the physical problem. However, considering the MPM was able to make a good simulation even without these refinements just comes to the advantage of the method.

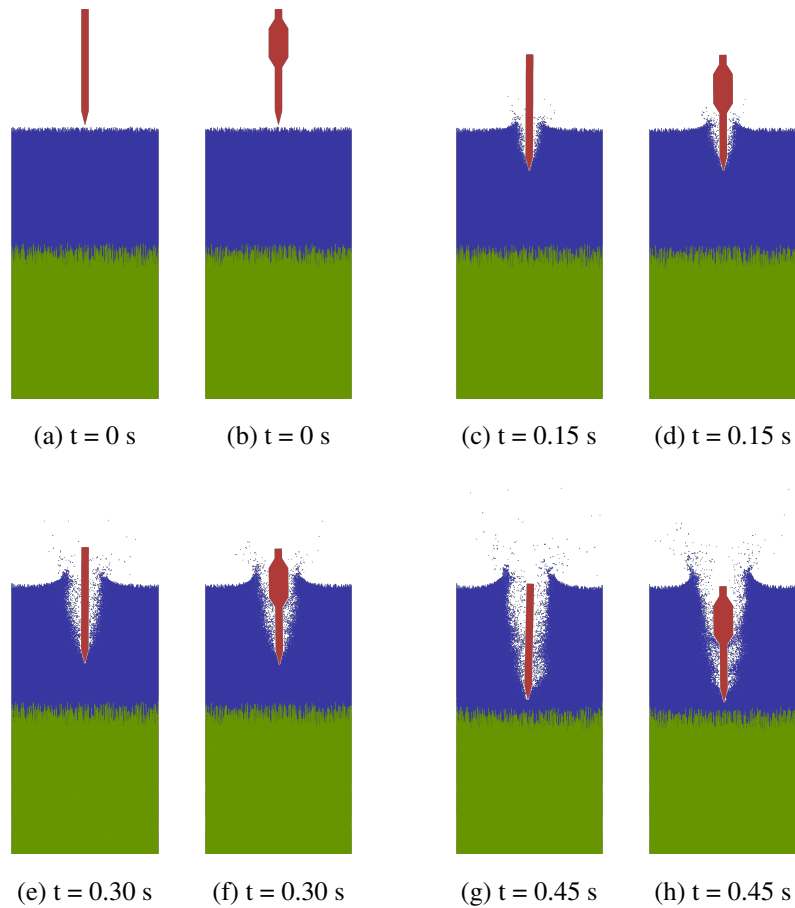


Figure 7. Comparison of torpedo anchors 1 and 2 at different time steps

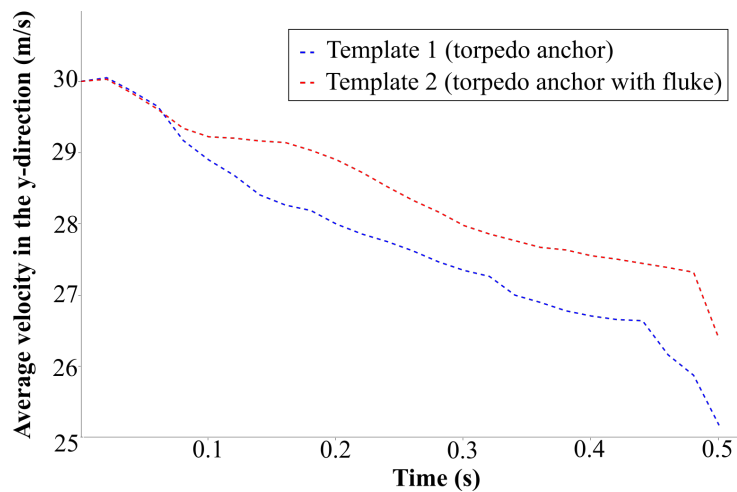


Figure 8. Velocity drop during torpedo anchor installation

## Acknowledgements

Our thanks to CENPES/PETROBRAS for the funding, to the Laboratory of Scientific Computing and Visualization (LCCV) for the infrastructure and to the researchers that are part of it, specially Ricardo Albuquerque Fernandes, who was responsible for the plasticity module, and Diogo Tenório Cintra, who was responsible for the development of the visualization module in the program which was used in the simulations of this article.

## References

- [1] Medeiros Júnior, C. J., 2002. Low Cost Anchor System for Flexible Risers in Deep Waters. In *Offshore Technology Conference*, Houston, Texas.
- [2] Bezerra, C. M. N., 2017. Análise numérica de cravação de estacas torpedo modeladas por integral de pressões. Master's thesis, Universidade Federal do Rio de Janeiro, Rio de Janeiro.
- [3] Carvalho Júnior, H., Cintra, D. T., Ramos Júnior, A. S., Silveira, E. S. S., Lira, W. W. M., Lages, E. N., & Ramos, V. C. L., 2005. Simulação do lançamento e cravação de estacas-torpedo em solo marinho com a utilização do Método dos Elementos Discretos. In *Proceedings of the XXVI Iberian Latin-American Congress on Computational Methods in Engineering – CILAMCE 2005*, Guarapari, ES.
- [4] Sousa, J. R. M., Aguiar, C. S., Ellwanger, G. B., Porto, E. C., Foppa, D., & Medeiros Júnior, C. J., 2011. Undrained Load Capacity of Torpedo Anchors Embedded in Cohesive Soils. *Journal of Offshore Mechanics and Arctic Engineering*, vol. 133, n. 2, pp. 021102.
- [5] Nazem, M., Carter, J. P., Airey, D. W., & Chow, S. H., 2012. Dynamic analysis of a smooth penetrometer free-falling into uniform clay. *Géotechnique*, vol. 62, n. 10, pp. 893–905.
- [6] Al-Kafaji, I. K. J., 2013. *Formulation of a dynamic material point method (MPM) for geomechanical problems*. PhD thesis, Universität Stuttgart.
- [7] Sulsky, D., Chen, Z., & Schreyer, H. L., 1994. A particle method for history-dependent materials. *Computer Methods in Applied Mechanics and Engineering*, vol. 118, pp. 179–196.
- [8] Jassim, I., Hamad, F., & Vermeer, P., 2011. Dynamic material point method with applications in geomechanics. In *Comgeo II*, number 1964.
- [9] Andersen, S. M. & Andersen, L. V., 2009. Material-Point-Method Analysis of Collapsing Slopes. *First International Symposium on Computational Geomechanics (COMGEO I)*, pp. 817–828.
- [10] Zhang, X., Chen, Z., & Liu, Y., 2017. *The Material Point Method*. Elsevier, 1st edition.
- [11] Bardenhagen, S. G., 2002. Energy conservation error in the material point method for solid mechanics. *Journal of Computational Physics*, vol. 180, n. 1, pp. 383–403.
- [12] York, A. R., Sulsky, D., & Schreyer, H. L., 1999. The material point method for simulation of thin membranes. *International Journal for Numerical Methods in Engineering*, vol. 44, n. 10, pp. 1429–1456.
- [13] Souza Neto, E. A., Perić, D., & Owen, D. R. J., 2008. *Computational Methods for Plasticity: theories and applications*. Wiley.
- [14] Awwad, T. & Al Kodsi, S., 2017. A comparison of numerical simulation models to determine the location of neutral plane. In *ICSMGE 2017 - 19th International Conference on Soil Mechanics and Geotechnical Engineering*.